Diamond & Related Materials 121 (2022) 108750

Contents lists available at ScienceDirect

Diamond & Related Materials

journal homepage: www.elsevier.com/locate/diamond

Separation of propylene from propane and nitrogen by Ag(I)-doped nanoporous carbons obtained from hydrothermally treated lignin

Dipendu Saha [a,*], Marisa Comroe [a], Rajamani Krishna [b], Margaret Rascavage [a], Joel Larwa [a], Victor You [a], Griffin Standhart [a], Brandon Bingnear [a]

[a] Department of Chemical Engineering, Widener University, One University Place, Chester, PA 19013, United States of America
[b] Van't Hoff Institute for Molecular Sciences, University of Amsterdam, Science Park 904, 1098 XH Amsterdam, the Netherlands

ARTICLE INFO

Keywords:
Adsorption
Porous carbon
Gas separation

ABSTRACT

Separation of propylene (C_3H_6) from propane (C_3H_8) is highly important to produce polymer (polypropylene)-grade C_3H_6. The separation of C_3H_6 from nitrogen (N_2) is also industrially important to recover unreacted propylene from the polypropylene plant. Compared to the cryogenic separation that is usually employed to separate C_3H_6, an adsorption process is sustainable and inexpensive provided a suitable adsorbent is developed. Lignin is an inexpensive, sustainable, and natural precursor of porous carbons. In this work, we have hydrothermally treated lignin followed by its carbonization, activation and Ag(I) doping to synthesize the Ag(I)-functionalized microporous carbons. These carbons were characterized with pore textural properties, scanning electron microscopic imaging (SEM), EDX-mapping, and X-ray photoelectron spectroscopy (XPS). The Ag(I)-doped nanoporous carbons possessed the BET surface areas of 440–1146 m^2/g and Ag(I) contents 1.5–5.9 at. %. The adsorption isotherms at 298 K and pressure upto 760 Torr suggested that all the adsorbents were selective to C_3H_6 compared to C_3H_8 and N_2. Ideally adsorbed solution theory (IAST) was employed to calculate the selectivity of binary mixtures of 50/50 C_3H_6/C_3H_8 and 30/70 C_3H_6/N_2 mixtures at 298 K. The selectivity of C_3H_6/C_3H_8 lies within 3–7 whereas the selectivity of C_3H_6/N_2 lies within 259–2600 that is higher than that of a large number of adsorbents reported in the literature. It is observed that the carbon with a lower Ag(I) content is more selective to C_3H_6 that may be attributed to the competition between Ag(I) and oxygen functionalities. The fixed-bed dynamic breakthrough simulations suggested that C_3H_6 can be separated from N_2 by all the carbons whereas C_3H_6 can be separated from C_3H_8 by the carbon with a lower Ag(I) content. The overall results suggested these carbons can potentially be used for C_3H_6 separations.

1. Introduction

Separation of light olefins from paraffins is one of the key separation needs of the modern world. Two important olefins that need to be separated from their paraffin counterparts are ethylene and propylene, which need to be separated from ethane and propane, respectively. The key use olefins in the plastic or polymerization industries, where ethylene and propylene are employed as the monomers for polyethylene and polypropylene, respectively. Light olefins have been produced over 200 million tons [1] worldwide with the market value of $ 254.6 billion in 2016; it is expected to reach $ 475.8 billion by the end of 2023 [2]. The global production of olefins can be approximated as 30 kgs of olefin per person on earth. Owing to the demand from developing countries, in the last decade, the olefin production has increased over 50%. The light olefins are produced by steam cracking of naphtha or C2/C3 paraffins [3,4]. The thermodynamics of the process limits the conversion to 20–40% and therefore, it is necessary to separate the olefins from the pool of the product mixtures. In order to obtain polymer-grade olefin, the purity of the olefins must be greater than 99.95%.

Propylene (C_3H_6) is one such olefin that need to be separated from propane (C_3H_8). Currently, the state-of-the-art separation strategy is cryogenic distillation. Owing to the small difference in boiling point of propane and propylene (propane: −42 °C; propylene: −47.6 °C, at ambient pressure) [5], it is possible to separate those olefins and paraffins by cryogenic distillation, however, the distillation must be carried out an extreme condition of −30 °C/3 bar. The process of cryogenic distillation is extremely costly, hazardous and not sustainable. In 1991, the cost of a single dedicated cryogenic unit was over $ 500 million [6]

* Corresponding author.
E-mail address: dsaha@widener.edu (D. Saha).

https://doi.org/10.1016/j.diamond.2021.108750
Received 23 June 2021; Received in revised form 8 November 2021; Accepted 27 November 2021
Available online 30 November 2021

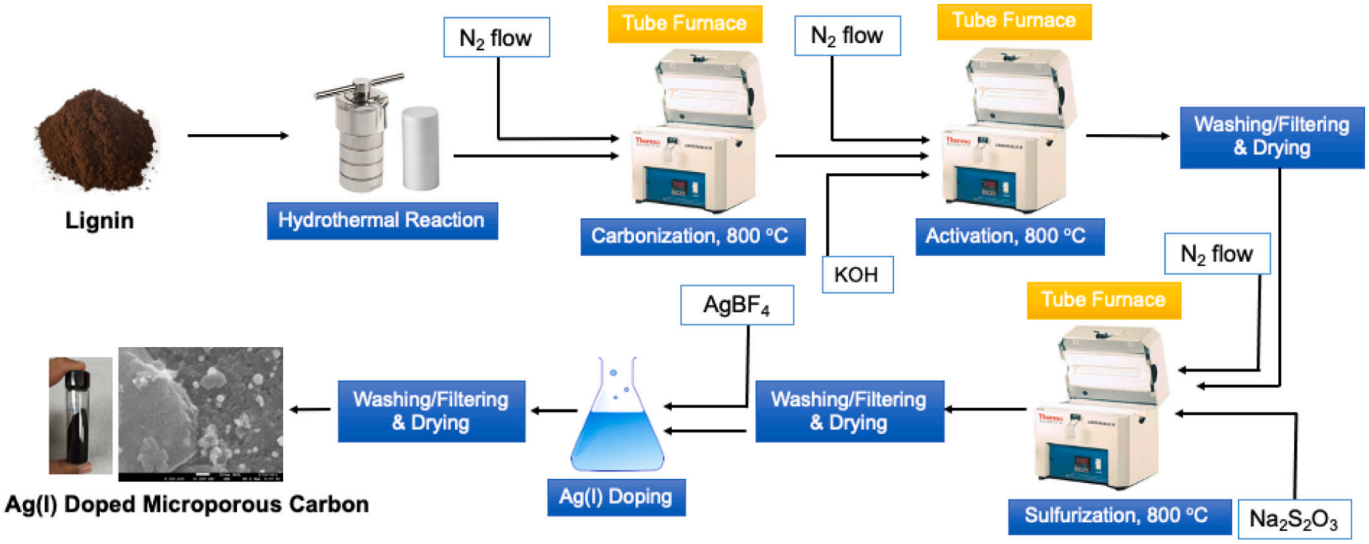

Fig. 1. Schematic of synthesis of Ag(I)-doped nanoporous carbon from Lignin.

and increased significantly in today's economy. The operation of this distillation is highly energy intensive; it utilizes about 0.12 quads (1 Quad = 10^{15} BTU) of energy annually in 1991 [7], which is equivalent to 0.3% of global energy usage. In the last 70 years, no improvement has been made in the propane-propylene separation [6].

Therefore, it is imperative to mention that adsorption could be an inexpensive and sustainable alternative to the cryogenic distillation. However, in order to implement the adsorption in such type of separation, a suitable adsorbent must be developed that is selective to either olefin or propylene. With time, several types of olefin-selective adsorbents have been developed and reported for propane-propylene separation, including Metal-organic frameworks [8], zeolites [9], functionalized silica [10], carbon molecular sieves (CMS) [11] [12], and nanoporous carbons [5]. One of the important strategies to increase the selectivity of the adsorbents to the olefins is to introduce selected metal ions, like Ag(I) or Cu(I) to the adsorbent surface that can selectively bind to the olefin, like propylene by so-called pi complexation.

There is need for separation of propylene from nitrogen as well. Upon polymerization of propylene to solid polypropylene, unreacted propylene is purged by N_2 gas creating a gas mixture consisting of 70% N_2 and 30% propylene. Currently, there is no economically viable way to separate propylene from the mixture; it is usually sent as vent gas to flare stack for burning in air. Although the loss of propylene in this process does not count to more than 1–2% of the original feed, the global total loss of propylene may add up to 2000–4000 tons/ year, which may be significant from economical point of view [13]. An analysis [14] suggested that the total global annual loss can be approximated as 1.5 million dollars combining the cost of both propylene and N_2. Furthermore, production of CO_2 owing to the burning of propylene also contributes to the global warming. In order to provide a suitable solution to this problem, several methods have been suggested to propylene recovery [15], including absorption, liquefaction, cryogenic distillation [16], membrane process [17,18], and adsorption [19,20]. Adsorption has gained lot of interest due to the inexpensive and sustainable nature of the process.

Despite several articles were published on MOF-based adsorbents for propylene separation, application of functionalized carbon-based materials is very limited [5]. In this work, we have synthesized Ag(I)-doped microporous carbons from lignin as carbon precursor. Lignin is the second largest biopolymer available in nature. It is highly inexpensive, non-hazardous and natural precursor of many carbon-based materials. It is the by-product of pulp and paper industries and biorefineries. Except few specific usages, there is no large-scape application of lignin as of today; most of the lignin is used as low-cost and low-calory fuel in the same industry where it has been generated. Utilization of lignin in the production of nanoporous carbons for gas separations [21] not only helps the economy of those industries but also create a sustainable route of synthesizing adsorbents from natural sources. In addition to incorporating lignin, we also employed a prior hydrothermal treatment or hydrothermal carbonization (HTC) that further increases sustainability of the process. A prior hydrothermal treatment of the biobased materials increases the char yield and hence decreases the emission of greenhouse CO_2 in the course of carbonization.

2. Experimental

2.1. Synthesis of Ag(I)-doped microporous carbons

The de-alkaline lignin was obtained from commercial sources (TCI America). At first, lignin was hydrothermally treated in a Teflon lined stainless reactor (Baoshishan). Typically, 15 g lignin and 44 mL water were introduced in the reactor and it was placed in a Vulcan 3–550 muffle furnace. The furnace was heated to 220 °C at the ramp rate of 5 °C/min for 24 h. Upon cooling, the hydrothermally treated lignin was taken out from the reactor and dried in 100 °C in a box furnace overnight. After that, it was carbonized within a porcelain boat at 800 °C with the ramp rate of 10 °C/min. The carbonization was performed in the Lingburg-Blue™ tube furnace and under the N_2 flow. The N_2 flow was continued till it is cooled to room temperature. After that, it was activated with potassium hydroxide (KOH). Typically, the carbonized lignin was mixed with solid KOH in 1:2 and 1:4 ratio and heated under N_2 flow within an alumina boat inside the tube furnace upto 800 °C and at a ramp of 10 °C/min and then cooled down to room temperature under the same N_2 flow. After that, the activated and lignin-derived carbon was washed several times with DI water, filtered and dried. After activation, each of the carbons were sulfurized with sodium thiosulfate ($Na_2S_2O_3$) as the precursor of sulfur. Typically, both the carbons were mixed with $Na_2S_2O_3$ in 1:4 ratio (1 g of KOH activated carbon with 4 g of $Na_2S_2O_3$). The mixtures of carbon and $Na_2S_2O_3$ were heated within the porcelain boat under N_2 flow and in the same tube furnace at a temperature of 800 °C and with a ramp rate of 10 °C/min. After cooling under N_2, it was washed several times of DI water, filtered and dried.

In order to perform the Ag(I)-doping, 1.0 g of each of the sulfurized carbons were dispersed in 20 mL DI water with 4 g $AgBF_4$ (99%, sigma-Aldrich) and stirred overnight. After that, the carbons were allowed to

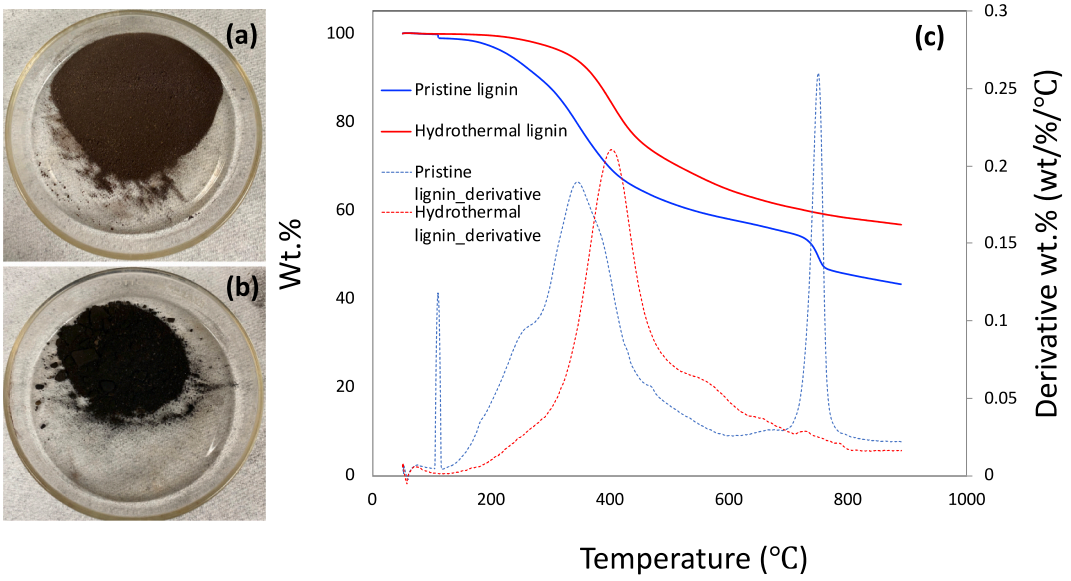

Fig. 2. Optical image of pristine lignin (a), hydrothermally treated lignin (b) and thermogravimetric analysis (TGA) of pristine and hydrothermally treated lignin (c).

settle, the water was decanted and a new batch of the same amounts of $AgBF_4$ and DI water were added to each of the carbon samples and stirred overnight. After that, the carbons were washed with DI water, filtered and dried. The carbons that were produced with 1:2 and 1:4 ratio of C/KOH were named as Ag—C1 and Ag—C2, respectively. The overall schematic of synthesis of Ag(I)-doped carbons were shown in Fig. 1.

2.2. Characterization of Ag(I)-doped microporous carbons

The Ag(I)-doped carbons were characterized with pore textural properties and material characteristics. The pore textural properties including BET surface area, total pore volume and pore size distributions were obtained in Quantachrome's Autosorb iQ-Any gas instrument by analyzing N_2 adsorption isotherms at 77 K and CO_2 adsorption isotherms at 273 K. Materials characteristics include scanning electron microscopic imaging (SEM) coupled with energy dispersive X-ray (EDX) and X-ray photoelectron spectroscopy (XPS). SEM and EDX were performed in a FEI Quanta 600 FEG Mark II Environmental Scanning Electron Microscope (ESEM). XPS data were collected in a Thermo-Fisher K-alpha instrument using an *AlKα* x-ray source (1486.7 eV) and with an overall resolution of 0.7 eV. Charge compensation was performed by using a combination of low energy electrons and ions.

2.3. Gas adsorption and separation by Ag(I)-doped microporous carbons

The gas adsorption isotherms, including that of C_3H_6, C_3H_8 and N_2 were measured in the same Autosorb iQ-Any Gas instrument at 298 K and pressure upto 760 Torr. All the gases were of ultra-high purity (UHP) grade or higher. The temperature was maintained by an external chiller (Julabo). The kinetic data of the gases were obtained in the same instrument under vector dose mode.

3. Results and discussions

3.1. Materials characteristics

Fig. 2(a) and (b) show the images of pristine and hydrothermally treated lignin, respectively. It is observed that the dark brown color of the lignin is changed to black upon hydrothermal treatment. One of the

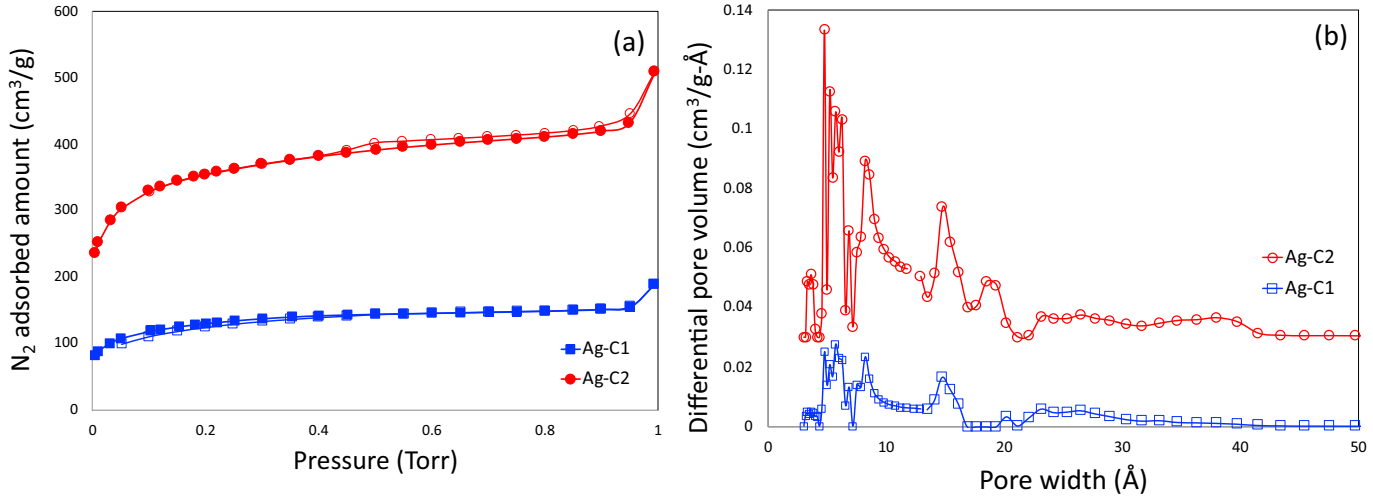

Fig. 3. Nitrogen adsorption-desorption isotherms at 77 K (a) and pore size distributions (b) of Ag—C1 and Ag—C2.

Table 1
Pore textural properties of Ag(I)-doped microporous carbons.

Adsorbent	BET surface area (m^2/g)	Micropore volume (cm^3/g)	Total pore volume (cm^3/g)
Ag-C2	1146	0.46	0.653
Ag-C1	440	0.15	0.232

key advantages of hydrothermal treatment of lignin can be observed in the thermogravimetric analysis (Fig. 2(c)). It is observed that the char yield of the hydrothermally treated lignin increases from around 43% to 57%, signifying that better stabilization of carbon and low emission of volatile matters are possible by hydrothermal treatment. In addition, two derivative peaks related to the mass loss in the temperatures of 111 °C and 751 °C in pristine lignin have completely disappeared in hydrothermally treated lignin. Furthermore, the largest derivative peak related to the mass loss at 348 °C in pristine lignin has been shifted to the higher temperature of 404 °C in the hydrothermally treated lignin. Such evidences confirmed that the hydrothermal treatment stabilizes the lignin thereby increasing its char yield. In addition, it needs to be mentioned that the process of synthesizing Ag-doped carbons from lignin is laborious and yield is approximately 0.02 g of Ag-doped carbon per gram of raw (as-received) lignin.

The N_2 adsorption-desorption isotherms at 77 K are shown in Fig. 3 (a). Both the isotherms of Ag—C1 and Ag—C2 type-I isotherms with negligible hysteresis of Ag—C2. The BET specific surface area of Ag—C1 and Ag—C2 are 440 and 1146 m^2/g, respectively. The total pore textural properties are shown in Table 1. It is evident that increasing C/KOH from 1:2 to 1:4 enhanced the surface area and pore volume of the resultant carbon. The non-local density function theory (NLDFT)-based pore size distribution (PSD) data of Ag—C1 and Ag—C2 are shown in Fig. 3(b), which are obtained by combining the individual PSD obtained from N_2 adsorption at 77 K (Fig. 3(a)) and CO_2 adsorption at 273 K [22–24], (Fig. S1 of supporting information.). As observed in Fig. 3(b), both the carbons have several pores within the micropore region. In supermicropore region, these carbons have the distinct pores at 18.5 and 14.75 Å. There are several pores in the ultramicropore region; the prominent ones are located in 8.2, 6.2, 5.2 and 4.78 Å. The pore width at around 3.6 Å is not a true pore, it is probably associated with the graphitic layer spacings. As already corroborated in the N_2 adsorption-desorption plot, the existence of mesopore is negligible in both the adsorbents.

The SEM-EDX imaging was performed only for the Ag—C2 as the representative in addition to the fact that it only demonstrated the significant propylene adsorption over propane (explained in details in

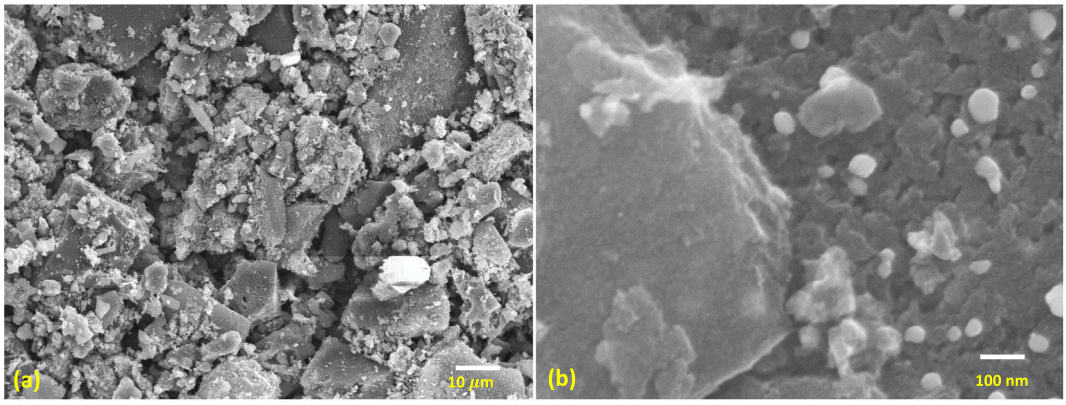

Fig. 4. SEM images of Ag—C2 in low magnification (a) and high magnification (b).

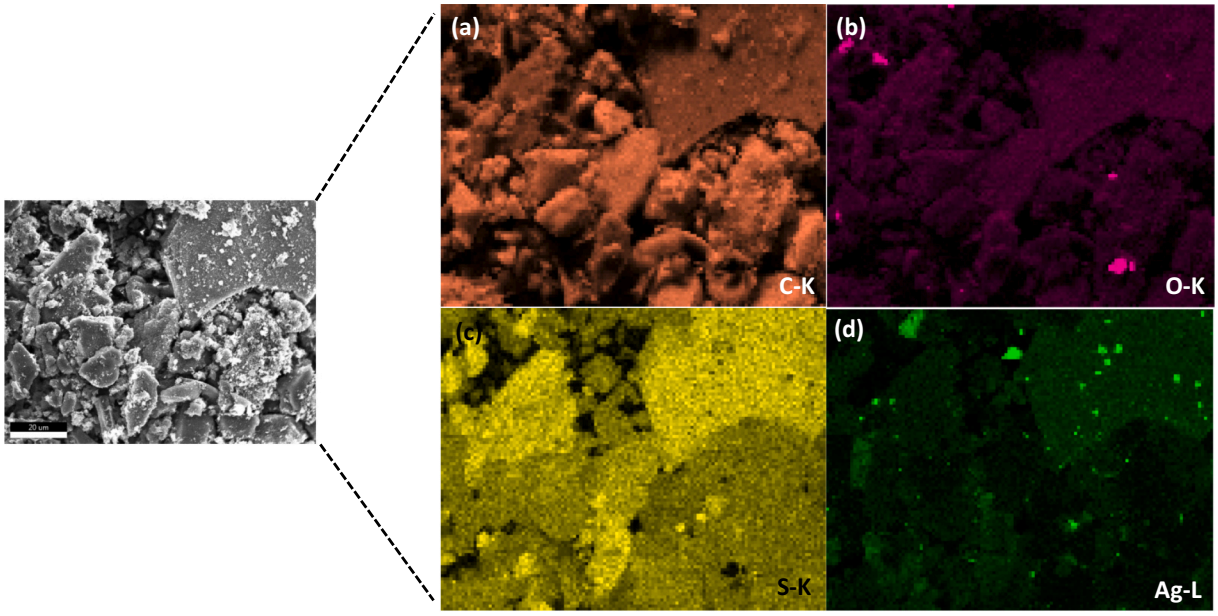

Fig. 5. EDX mapping of Ag-C2; Carbon (a), Oxygen (b), sulfur (c) and silver (d).

Table 2
Elemental compositions of Ag(I)-doped microporous carbons obtained by XPS.

Elements (at.%)	Ag-C1	Ag-C2
C	75.3	88.5
O	8.6	6.8
S	9.5	3.2
Ag	5.9	1.5
F	0.7	0.0

Section 3). The SEM imaging results of Ag—C2 are shown in Fig. 4(a) and (b) for lower and higher magnifications, respectively. As observed in this figure, the shape and size of those particles are quite irregular. The larger particles are in the range of 30–50 μm where the size of the smaller particles was as small as 50–100 nm. The energy dispersive X-ray (EDX) results were shown in Fig. 5. The elemental mapping for carbon (C—K), oxygen (O—K), sulfur (S—K) and silver (Ag-L) confirmed the uniform distribution of those elements in this adsorbent. The EDX revealed that the elemental composition of C, O, S, and Ag are 87.0. 6.9, 4.5 and 1.2 at.%, respectively, which can be translated to 72.6, 7.7, 10.0 and 8.8 wt%, respectively. It should be noted that the EDX also found 0.5 at.% or 0.9 wt% Al, which might be originated from porcelain or alumina boat at high temperature in the course of synthesis. EDX plots of elemental contents are shown in Fig. S2 of supporting information.

X-ray photoelectron spectroscopy (XPS) results revealed the elemental compositions and functionalities of Ag—C1 and Ag—C2. The elemental compositions of C, O, S and Ag in Ag—C1 and Ag—C2 are shown in Table 2 and the peak fitting results of C-1 s, O-1 s, S-2p and Ag-3d for Ag—C2 are shown in Fig. 6(a-d). Ag—C1 has a small amount of F (0.7 at.%) that may be originated from $AgBF_4$. The elemental percentages of Ag—C2 are very similar to what were obtained by EDX with slightly higher difference in sulfur contents (XPS-3.2 at.%, EDX-4.5 at.%) that might be caused by the slight heterogeneity in surface and bulk composition. The Ag(I) contents in Ag—C1 and Ag—C2 are 5.9 and 1.5 at.%, respectively. As the individual functionalities of Ag cannot be obtained from the Ag-$3d_{3/2}$ and -$3d_{5/2}$ results, we investigated the peak deconvolution results of the other elements. Since there was no satellite in Ag-3d peak, it can be concluded that metallic Ag is not present in the system. In a similar fashion, it can also be concluded that no oxides of Ag are present in these systems due to the absence of its signature in O-1 s peaks. From the results S-2p peak deconvolution and at the BE of 161.3 eV, it was found that Ag—C1 and Ag—C2 have the Ag—S functionalities in the range of 0.5 and 2.2 at.%, respectively. It clearly indicates that both the Ag(I) contents and Ag—S functionalities are directly correlated to the S content. It corroborates the key purpose of S-doping onto the carbons as the sulfurized surface increases the affinity of the carbon towards Ag. It is also well elaborated in our previous publication [5]. The remaining types of Ag(I) functionalities could not be detected by XPS. It is possible that Ag(I) has been adsorbed in the surface or pores of the carbon matrix.

As mentioned, Ag—C1 has higher oxygen content than that of Ag—C2 (Ag-C1: 8.6 at.%, Ag-C2: 6.8 at.%). There are two distinct peaks that can be deconvoluted are in the BE levels of ~531.2 and 533 eV. The

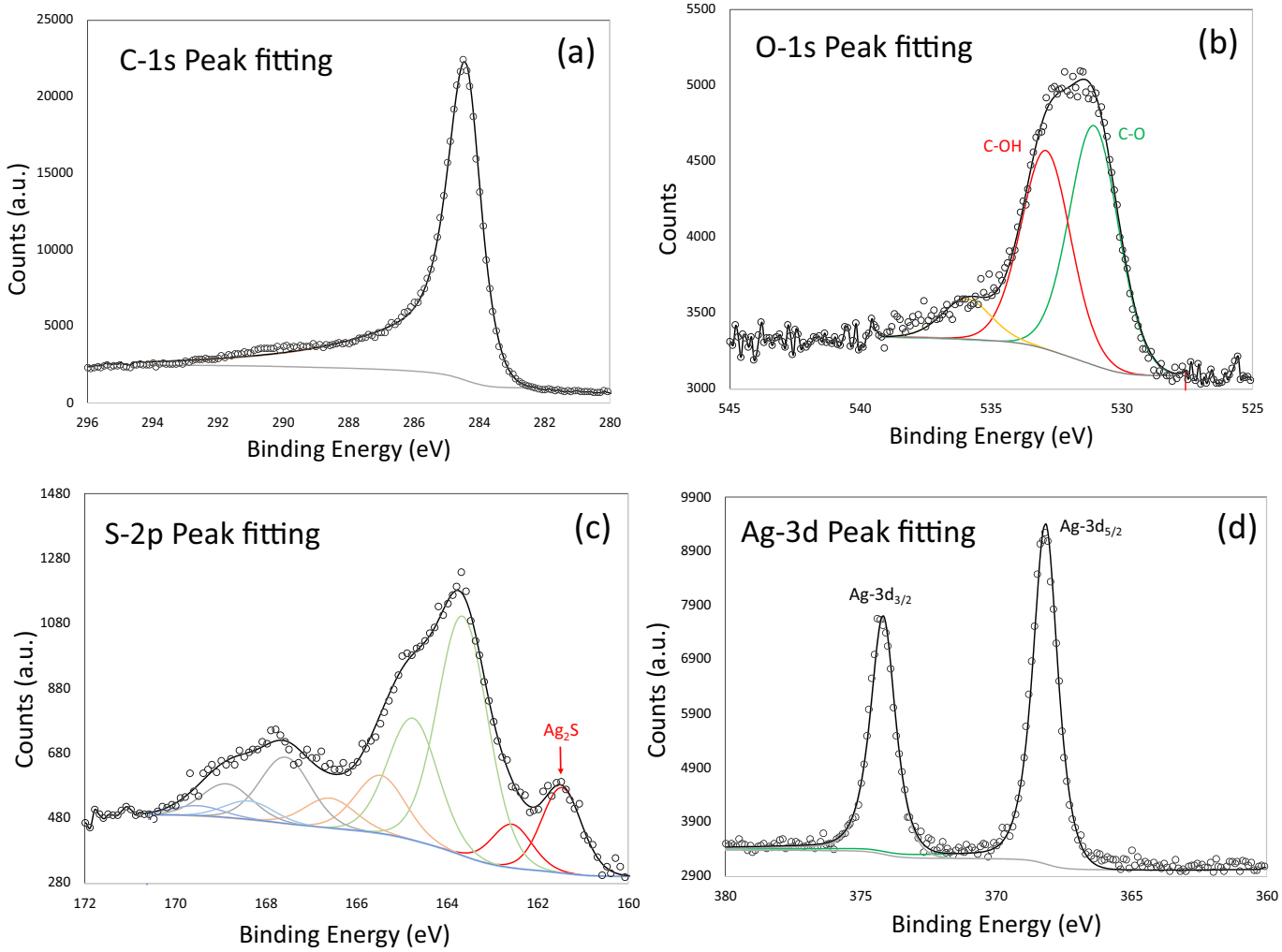

Fig. 6. XPS peak fitting results of Ag—C2 for C-1 s (a), O-1 s (b), S-2p (c) and Ag-3d (d).

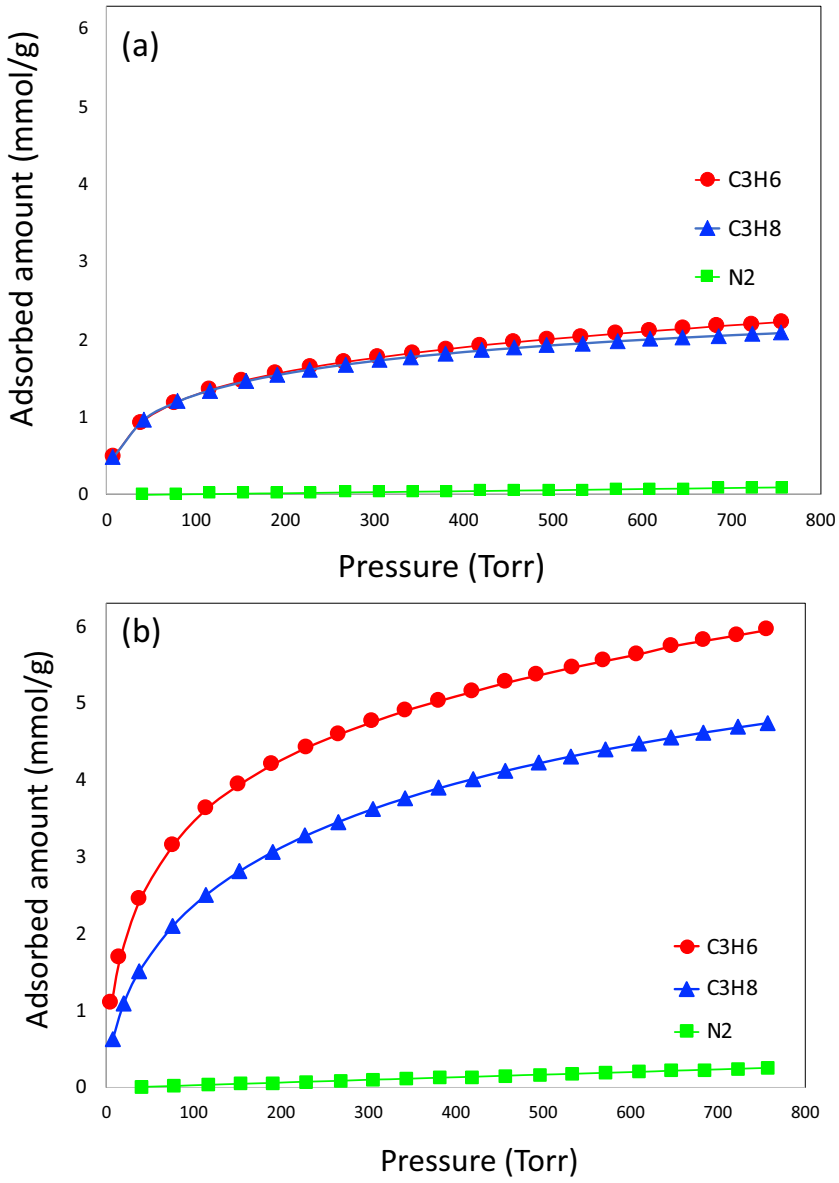

Fig. 7. C_3H_6, C_3H_8 and N_2 adsorption isotherms at 298 K for Ag—C1 (a) and Ag-C2(b).

oxygen functionality at 531.2 eV can be attributed to C—O functionality whereas the peak at ~533 eV may represent C—O or C-O-C functionality. Those two peaks consist of 50.2 and 41.4% of total oxygen contents for Ag—C1 and 68.1 and 27.4% for Ag—C2. It is observed that the peak fitting results for C-1 s are very similar for both adsorbents, except Ag—C1 possesses more functionalities in the region of 288–292 eV region. Although those regions may be attributed to the C═O or O-C=O functionalities as depicted in the previous publications [25] [26], they may also contribute to the plasmon loss for sp^2-carbon-based materials and there is no known way to isolate them from the other functionalities. Therefore, we did not make a deliberate attempt quantify the representative carbon functionalities from the C-1 s peaks.

3.2. Adsorption and separation of gases

Adsorption isotherms of C_3H_6, C_3H_8 and N_2 at 298 K are shown in Fig. 7 for both Ag—C1 and Ag—C2. It is obvious that N_2 adsorbed amounts in both the samples are lower compared to that of C_3H_6 thereby making them suitable C_3H_6/N_2 separation. C_3H_6 and C_3H_8 adsorbed amounts are very similar for Ag—C1 that suggests that Ag—C1 is not suitable for C_3H_6/C_3H_8 separation. However, a different scenario is observed for Ag—C2. C_3H_6 adsorbed amount (6 mmol/g) in substantially higher compared to that of C_3H_8 (4.5 mmol/g) at 760 Torr pressure and it makes Ag—C2 suitable for C_3H_6/ C_3H_8 separation as well. It is also noticeable that equilibrium adsorption amounts of all the gases are much higher in Ag—C2 compared to that Ag—C1 that can be attributed the higher specific surface area and micropore volume of Ag—C2. Not only it is intuitive to elaborate that narrow micropores are suitable smaller molecules, like C_3H_6 or C_3H_6, we have also recently demonstrated such phenomena by density function theory (DFT) [27]. The equilibrium uptake capacity of C3 hydrocarbons in our study is higher than carbon molecular sieves [11,12], Ag-doped silica [10,28,29], zeolites, like NaX [30], boron nitride [31], and different other MOFs, like Co-MOF-74 [30], FeMIL-100 [30], MUV-3(Fe) [32], ZIF-8 (Zn) [32] and ZIF-67(Co) [32,33].

Influence of Ag(I) in facilitating the olefin adsorption over paraffin by π- complexation has also been well documented. When a specific metallic ion, like Ag(I) comes in contact with an olefin, π-orbital of olefin and *s*- or *d*-orbital of become partially overlapped. The filled π orbital of olefin overlaps with the empty *s* orbital of the metal ion and electron

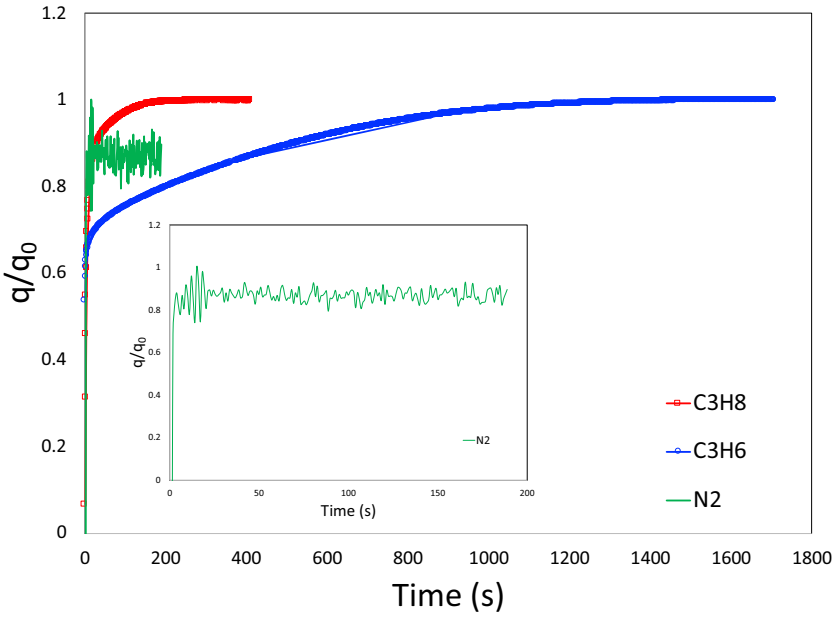

Fig. 8. C_3H_6, C_3H_8 and N_2 adsorption kinetics on Ag—C2 at 298 K. The inset plot shows the kinetics of N_2.

donation takes place from olefin towards metal ion. At the same time, the *d* orbital of the metal ion overlaps with the π* antibonding orbital of olefin that results in a backdonation of electrons from *d*-orbital towards π* antibonding orbital. This type of interaction partially loosens the C—C bond of olefins but the overall molecular entity of olefins remains completely intact. The interactions between olefin and paraffin in Ag(I)-doped carbon surface have also been investigated by DFT [27]. It was demonstrated that Ag(I) forms bond with propylene with bond distances of 2.37 and 2.32 Å for the two carbons forming the π bond within the narrow slit shaped pore. However, in the presence of propane, it was observed that Ag(I) has the tendency to form *π* bonds with carbon atoms present on the opposite side of the pore wall thereby rejecting the propane molecule. Such interactions of Ag(I) functionalities with olefins have also been confirmed by molecular orbital (MO) analysis [27].

As observed in XPS data, Ag—C1 has more Ag(I) content (5.9 at.%) compared to that of Ag—C2 (1.5 at.%). As π complexation is caused by Ag(I) alone, it is not intuitive to observe that Ag—C2 prefers C_3H_6 adsorption over C_3H_8 but Ag—C1 does not. Such anomalous results may be caused by other functionalities on the carbon surface. As observed in the XPS, Ag—C1 has higher oxygen contents compared to that of Ag—C2, including C-OH and C-O/O-C-O type of functionalities. It has been reported in the literature [34] [35], that those type of O-bearing functionalities prefer a paraffin over olefin on the carbon surface by possibly shortening the bond distance between the paraffin and carbon. Besides that, a stronger Van der Waals force between paraffin and the carbon surface also supports the favorable adsorption of paraffin on the carbon surface. Although such incidents were all reported for higher selectivity of ethane compared to that of ethylene on oxygen functionalized carbon surface, we hypothesize that such occurrences may also play a crucial role in propane adsorption and the competition between Ag(I) and oxygen bearing functionalities that resulted in the similar adsorbed amounts for propane and propylene on Ag—C1. Although the carbons also have sulfur content in their matrices, it is very unlikely that sulfur will have any influence in the adsorption of alkane or alkene, like propane and propylene as observed in our previous publication [5].

The linear isotherms can be fit with the well-known Henry's law and given as

$$q = kp \tag{1}$$

where q and p are the adsorbed amounts (mmol/g) and pressure (p), respectively, and k is the Henry's constant. The N_2 adsorption isotherms were modeled with Henry's law and Henry's constant for Ag—C1 and Ag—C2 are given as 1.0×10^{-4} and 3.0×10^{-4} mmolg^{-1} Torr^{-1}, respectively.

The Sips or Langmuir-Freundlich model is a type of universal adsorption isotherm model that can fit most of the adsorption isotherms. The Sips isotherm model is given as

$$q = q_{sat}\frac{bp^{\upsilon}}{1 + bp^{\upsilon}} \tag{2}$$

where, b, q_{sat} and υ are the fitting constants. The constants are shown in Tables S1 and S2 of supporting information.

The kinetics of C_3H_6, C_3H_8 and N_2 are shown in Fig. 8. It is clear that the kinetics of N_2 adsorption is very fast, it reached the saturation within few seconds only. It is observed that kinetics of C_3H_8 is much faster compared to that of C_3H_6; C_3H_8 reached saturation within 200 s, whereas it took about 1200 s for C_3H_6 to reach the saturation. The adsorption kinetics may be fitted by the micropore diffusion model [36]

$$\frac{q}{q_e} = 1 - \frac{6}{\pi^2}\sum_{n=1}^{n=\infty}\frac{1}{n^2}exp\left(\frac{n^2\pi^2 D_c t}{r_c^2}\right) \tag{3}$$

where $q(t)$ is the adsorbed amount at time t, q_e is the saturated adsorbed amount, D_c is the intracrystalline diffusivity and r_c is the intracrystalline radius. It is a practice in literature to model fit the adsorption kinetics data with the first term of the summation only and the resultant equation becomes

$$\frac{q}{q_e} = 1 - \frac{6}{\pi^2}exp\left(\frac{\pi^2 D_c t}{r_c^2}\right) \tag{4}$$

The diffusive time constant (D_c/r_c^2, s^{-1}) can be calculated by the linear regression of logarithmic form of the equation within 75 to 99% of the saturation level. It is observed the diffusive time constants of N_2, C_3H_8 and C_3H_6 are 0.00399. 0.00192 and 0.00029 s^{-1}, respectively. It needs to be noted that the diffusive time constants of C_3H_6 is 1–3 orders of magnitude higher compared to that of Silica-chabazite zeolite (SiCHA) reported in literature [37].

As it is very difficult to perform the binary gas adsorption owing to the instrument requirements, it is a common practice to perform the pure component adsorption and report the selectivity values that can

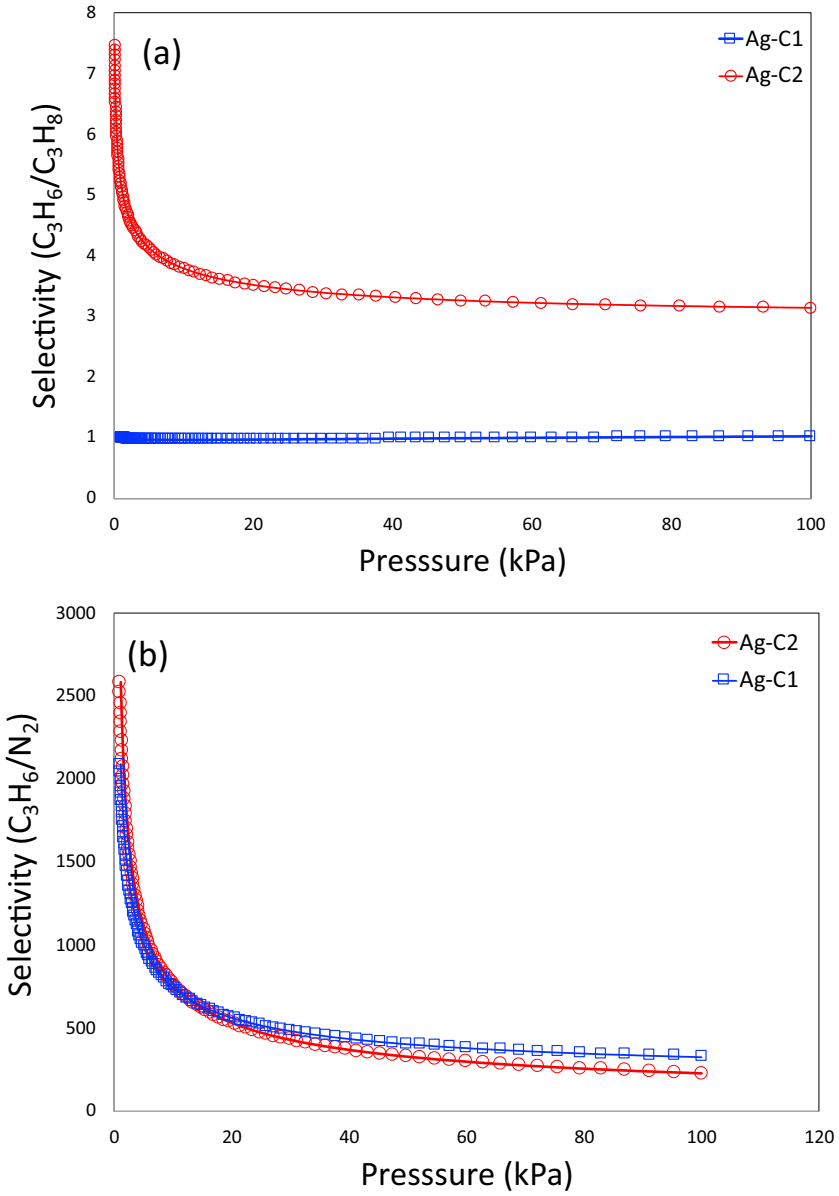

Fig. 9. IAST-based selectivities of C_3H_6/C_3H_8 (a) and C_3H_6/N_2 (b).

signify the possible separation of binary gas mixtures. The selectivity can be defined as

$$S_{ads} = \frac{q_1/q_2}{p_1/p_2} \tag{5}$$

where q_1, q_2 are the molar loadings (units: mmolg^{-1}) in the adsorbed phase in equilibrium with a gas mixture with partial pressures p_1, p_1 in the bulk gas. The component '1' is the preferred species whereas component '2' is the non-preferred component. It is a common practice to calculate the selectivity values from Ideally Adsorbed Solution Theory (IAST) from pure-component adsorption data. In this work, we calculated the selectivity of binary mixtures of 50/50 C_3H_6/C_3H_8 and 30/70 C_3H_6/N_2 mixtures in Ag—C1 and Ag—C2 at 298 K. The IAST-based selectivity values for C_3H_6/C_3H_8 and C_3H_6/N_2 in Ag—C1 and Ag—C2 are shown in Fig. 9(a-b). It is observed that both the adsorbents demonstrated high selectivity values for C_3H_6/N_2 separation, around 2600 to 250. The selectivity of C_3H_6/C_3H_8 in Ag—C2 are in the range of 7–3. As already suggested in the adsorption isotherms, Ag—C1 does not represent a favorable selectivity for C_3H_6/C_3H_8 separation.

It needs to be noted the IAST selectivity of C_3H_6/N_2 in these Ag(I)-doped carbons is much higher compared to that of several MOF-based materials reported in literature [20]. In a study, Tan et al. [20] examined 8 MOFs, including CAU-1, UiO-66, UiO-66-NH_2, PCN-222, MIL-101, MIL-101-NH_2, MOF-808 and ZIF-8. The highest selectivity of C_3H_6/N_2 at 298 K belonged to CAU-1, which is not more than 300–175.

The kinetic selectivities (S_k) may be represented as the ratio of diffusive time constants of the two gases [31,38],

$$S_K = \frac{\left(\frac{D_c}{r_c^2}\right)_i}{\left(\frac{D_c}{r_c^2}\right)_j} \tag{6}$$

where, i and j are the faster and slower adsorbing species, respectively. The kinetic selectivities of N_2/C_2H_6 and C_2H_8/C_2H_6 in Ag—C2 are 13.55 and 6.52, respectively. The kinetic selectivity of C_2H_8/C_2H_6 is higher than that of TO, DTO and ground DBTO-based MOFs, but lower than that of BTO and DBTO-based MOFs [38].

The performance of industrial fixed bed adsorbers is dictated by a

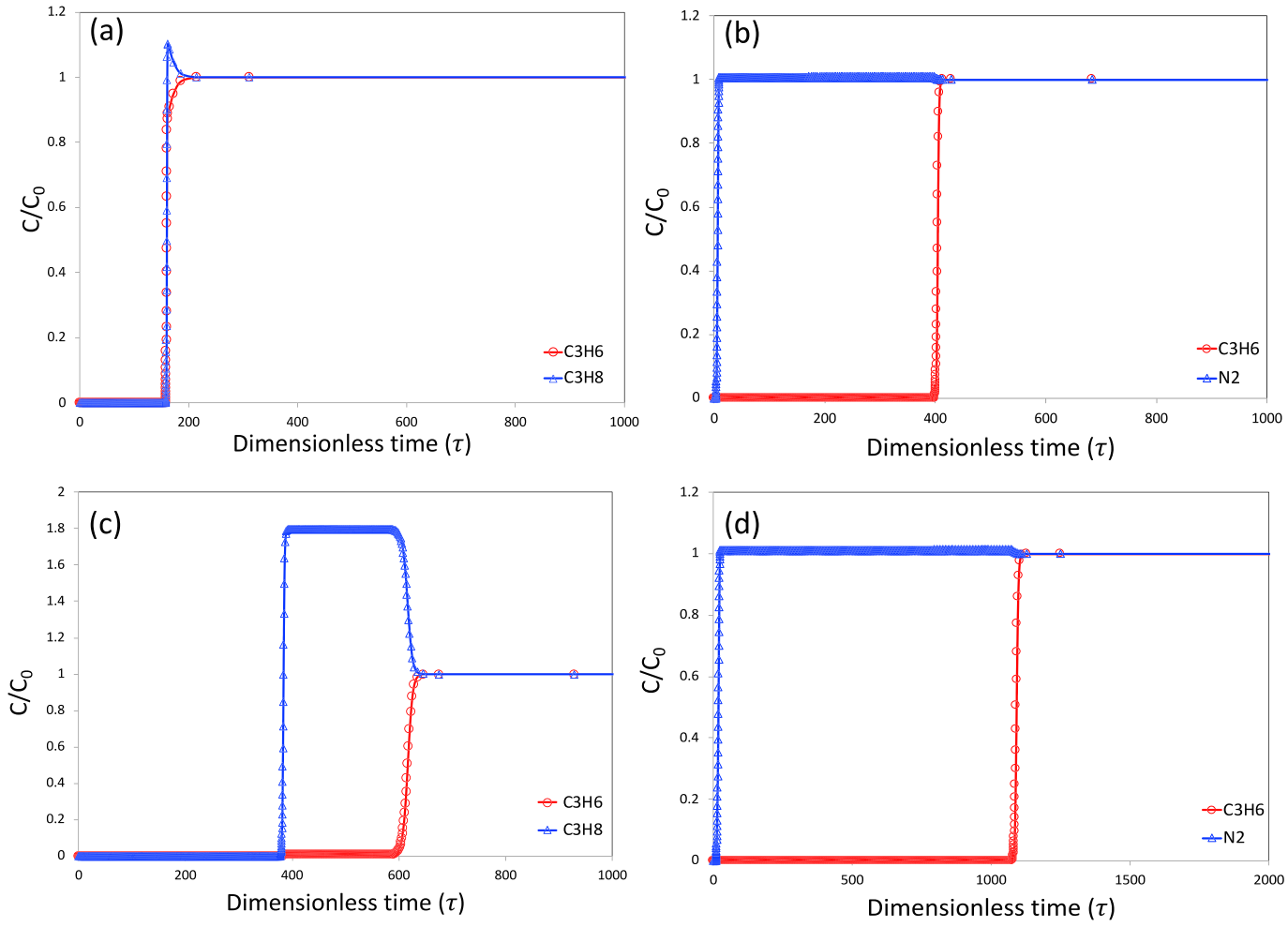

Fig. 10. Simulated breakthrough plots of C_3H_6/C_3H_8 and C_3H_6/N_2 for Ag—C1 (a-b) and Ag—C2 (c-d).

combination of adsorption selectivity and uptake capacity. Transient breakthrough simulations were carried out for binary 50/50 C_3H_6/C_3H_8 and 30/70 C_3H_6/N_2 mixtures in Ag—C1 and Ag—C2, operating at a total pressure of 100 kPa and temperature 298 K, using the methodology described in earlier publications [39–42]. The breakthrough simulations were carried out using in-house custom-built code. For the breakthrough simulations, the following parameter values were used: length of packed bed, $L = 0.3$ m; void fraction of packed bed, $\varepsilon = 0.4$; superficial gas velocity at inlet, $u = 0.04$ m/s. The breakthrough simulation results were shown in Fig. 10(a-d). In those figures, the x-axis is the dimensionless time, $\tau = \frac{tu}{L\varepsilon}$, defined by dividing the actual time, t, by the characteristic time, $\frac{L\varepsilon}{u}$. The y-axis is the dimensionless concentrations of each component at the exit of the fixed bed, normalized with respect to the inlet feed concentrations. It is observed that there is a large difference in dimensionless time between the breakthrough of C_3H_6 and N_2 from the fixed-bed adsorption columns for both Ag—C1 and Ag—C2 thereby suggesting that both the adsorbents can separate C_3H_6/N_2 mixtures. However, a different scenario was observed for C_3H_6/C_3H_8 separation. Large difference in dimensionless time for the breakthrough of C_3H_6 and C_3H_8 in Ag—C2 confirmed that it can separate those two gases. However, there is no such difference in the dimensionless time for Ag—C1 suggesting that it cannot separate those two gases. It is also quite imperative to note that the trend in breakthrough time directly followed same trend for IAST-based selectivity values.

4. Conclusions

In this research, we have synthesized Ag(I)-functionalized microporous carbons from hydrothermally treated lignin. Sustainable fingerprints of the synthesis can be attributed to the utilization of lignin as an inexpensive, natural precursor as we well as lowering of CO_2 emission during the carbonization step owing to the prior hydrothermal treatment. The resultant carbons demonstrated the BET specific surface areas of 440–1146 m^2/g and micropore volume of 0.65–0.23 cm^3/g. SEM-EDX imaging confirmed the inform distribution of C, O, S and Ag within the carbon matrix. XPS analysis revealed that Ag(I) content was in the range of 1.5–5.9 at.% and all the Ag was present in Ag(I) form. All the carbons demonstrated higher C_3H_6 adsorbed amounts compared to that of N_2 suggesting they can separate those two gases. However, only one carbon demonstrated favorable selectivity towards C_3H_6 for C_3H_6/C_3H_8 separation. The selectivity towards C_3H_6 may be attributed to the π complexation between Ag(I) and π bond of propylene. A negligible selectivity towards C_3H_6 by a carbon with the highest Ag(I) content may be caused by the competition with the higher oxygen functionalities that may facilitate the C_3H_8 adsorption. The kinetics of adsorption suggested that N_2 adsorption is the fastest in the system, followed by C_3H_8 and C_3H_6. Finally, the breakthrough simulation confirmed that all the adsorbents can separate C_3H_6 and N_2, while one adsorbent can potentially separate C_3H_6 from C_3H_8.

CRediT authorship contribution statement

Dipendu Saha: Conceptualization, Project administration, Funding acquisition, Methodology, Investigation, Supervision, Formal analysis, Writing – original draft, Writing – review & editing. **Marisa Comroe:** Methodology, Investigation, Supervision, Writing – original draft. **Rajamani Krishna:** Methodology, Investigation, Formal analysis. **Margaret Rascavage:** Investigation. **Joel Larwa:** Investigation, Formal analysis. **Victor You:** Investigation. **Griffin Standhart:** Investigation, Resources. **Brandon Bingnear:** Investigation.

Declaration of competing interest

The authors declare that they have no known competing financial interests or personal relationships that could have appeared to influence the work reported in this paper.

Acknowledgement

This work was supported by American Chemical Society Sponsored Petroleum Research Fund (ACS-PRF), grant number 59667-UR10 (PI: D. Saha). M.C., M. R., J. L. and V. Y. acknowledges funding from School of Engineering of Widener University. The authors acknowledge Sylvie Rangan (Rutgers University) for XPS data fitting and Jamie Ford (University of Pennsylvania) for SEM-EDX.

Appendix A. Supplementary data

Supplementary data to this article can be found online at https://doi.org/10.1016/j.diamond.2021.108750.

References

[1] J.A. Moulijn, M. Makkee, A. van Diepen, Chemical Process Technology, John Wiley & Sons, Chichester, England, 2001.
[2] Light olefins market research report—forecast to 2023. https://www.marketresearchfuture.com/reports/light-olefin-market-1037 (Accessed June 2018).
[3] S. Matar, H. Hatch, L. F., Chemistry of Petrochemical Processes, 2nd ed., Gulf Publishing Company, Texas, 2000.
[4] J.A. Moulijn, M. Makkee, A. van Diepen, Chemical Process Technology, John Wiley & Sons, Chichester, England, 2001.
[5] D. Saha, B. Toof, R. Krishna, G. Orkoulas, P. Gismondi, R. Thorpe, M. Comroe, Separation of ethane-ethylene and propane-propylene in Ag(I)-doped and sulfurized microporous carbon, Microporous Mesoporous Mater. 299 (2020), 110099.
[6] R.Bruce Eldridge, Olefin/paraffin separation technology: a review, Ind. Eng. Chem. Res. 32 (1993) 2208–2212.
[7] J.L. Humphrey, Seibert, R.A. Koort, Separations Technologies Advances And Priorities, U.S. Department of Energy, 1991. Report 12920-1.
[8] Energy Chem. (1) (July 2019), 100006, https://doi.org/10.1016/j.enchem.2019.100006.
[9] C. Selzer, A. Warner, S. Kaskel, Selective adsorption of propene over propane on hierarchical zeolite ZSM-58, Ind. Eng. Chem. Res. 57 (2018) 6609–6617.
[10] M. Kargol, J. Zajac, D.J. Jones, T. Steriotis, P/ vitse, porous silica materials derivatized with Cu and Ag cations for selective propene−propane adsorption from the gas phase: aluminosilicate ion-exchanged monoliths, Chem. Mater. 16 (2004) 3911–3918.
[11] J. Liu, Y. Liu, D.K. Talay, E. Calverley, M. Brayden, M. Martinez, A new carbon molecular sieve for propylene/propane separations, Carbon 85 (2015) 201–211.
[12] J. Liu, E.M. Calverley, M.H. McAdon, J.M. Goss, Y. Liu, K.C. Andrews, T. D. Wolford, D.E. Beyer, C.S. Han, D.A. Anaya, R.P. Golombeski, C.F. Broomall, S. Sprague, H. Clements, K.F. Mabe, New carbon molecular sieves for propylene/propane separation with high working capacity and separation factor, Carbon 123 (2017) 273–282.
[13] A.M. Ribeiro, M.C. Compo, G. Narin, J.C. Santos, A. Ferreira, J.S. Chang, Y. K. Hwang, Y.-K. Seo, H.-H. Lee, J.M. Loueiro, A.E. Rodrigues, Pressure swing adsorption process for the separation of nitrogen and propylene with a MOF adsorbent MIL-100(Fe), Sep. Purif. Technol. 110 (2013) 101–111.
[14] M. Jacobs, D. Gottschlich, R.W. Baker, Monomer Recovery in Polyolefin Plants, Membrane Technology & Research Inc., 2000.
[15] H. Nishida K. Tsubohara E. Okamoto Y. Deguchi, Method of Reusing Exhaust Gas in Polymer Production Plant, US Patent 7,449,048 B2, 2008.
[16] D. Gottschlich M. L. Jacobs Monomer recovery process. U.S. Patent 5,769,927, 1998.
[17] M. Fang, H. Zhang, J. Chen, T. Wang, J. Liu, X. Li, J. Li, X. Cao, A facile approach to construct hierarchical dense membranes via polydopamine for enhanced propylene/nitrogen separation, J. Membr. Sci. 499 (2016) 290–300.
[18] I.G. Giannakopoulos, V. Nikolakis, Recovery of hydrocarbons from mixtures containing C3H6, C3H8 and N2 using NaX membranes, J. Membr. Sci. 305 (2007) 332–337.
[19] S.-S. Han, J.-H. Park, J.-N. Kim, S.-H. Cho, Propylene recovery from propylene/propane/nitrogen mixture by PSA process, Adsorption 11 (2005) 621–624.
[20] Q. Tan, Y. Peng, W. Xue, H. Huang, D. Liu, C. Zhong, Ultramicroporous metal-organic framework with polar groups for efficiently recovering propylene from polypropylene off-gas, Ind. Eng. Chem. Res. 58 (31) (2019) 14333–14339.
[21] D. Saha, G. Orkoulas, S.E. Van Bramer, H.-C. Ho, J. Chen, D.K. Hensley, CO2 capture in lignin-derived and nitrogen-doped hierarchical porous carbon, Carbon 121 (2017) 257–266.
[22] D. Saha, H.A. Grappe, Adsorption properties of activated carbon fibers, in: D. Chen (Ed.), Activated Carbon Fiber And Textiles, Ed.; Woodhead Publishing, 2017, pp. 143–165.
[23] D. Saha, B. Taylor, N. Alexander, D.F. Joyce, G.I. Faux, Y. Lin, V. Shteyn, G. Orkoulas, One-step conversion of agro-wastes to nanoporous carbons: role in separation of greenhouse gases, Bioresour. Technol. 256 (2018) 232–240.
[24] D. Saha, C.P. Richards, R.G. Haines, N.D. D'Alessandro, M.J. Kienbaum, C. A. Griffaton, Competitive adsorption of lead in sulfur and iron dual-doped mesoporous carbons, Molecules 25 (2020) 403.
[25] D. Saha, Y. Li, Z. Bi, J. Chen, J.K. Keum, D.K. Hensley, H.A. Grappe, H. Meyer III, S. Dai, M.P. Paranthaman, A.K. Naskar, Studies on supercapacitor electrode material from activated lignin derived mesoporous carbon material, Langmuir 30 (2014) 900–910.
[26] D. Saha, R. Thorpe, S.E. Van Bramer, N. Alexander, D. Hensley, G. Orkoulas, J. Chen, Synthesis of nitrogen and sulfur co-doped nanoporous carbons from algae: role in CO2 separation, ACS Omega (2018) 18592–18602.
[27] G. DeLuca, D. Saha, S. Chakraborty, Why Ag(I) grafted porous carbon matrix prefers alkene over alkane?An inside view from ab-initio study, Microporous Mesoporous Mater. 316 (2021), 110940.
[28] C.A. Grande, J.D.P. Araujo, S. Cavenati, N. Firpo, E. Basaldella, A.E. Rodrigues, New π-complexation adsorbents for propane−propylene separation, Langmuir 20 (2004) 5291–5297.
[29] C.A. Grande, N. Firpo, N. Basaldella, A.E. Rodrigues, Propane/propene separation by SBA-15 and π-complexated Ag-SBA-15, Adsorption 11 (2005) 775–780.
[30] Y. He, R. Krishna, B. Chen, Metal–organic frameworks with potential for energy-efficient adsorptive separation of light hydrocarbons, Energy Environ. Sci. 5 (2012) 9107–9120.
[31] D. Saha, G. Orkoulas, S. Yohannan, H.-C. Ho, E. Cakmak, J. Chen, S. Ozcan, Nanoporous boron nitride as exceptionally thermally stable adsorbent: role in efficient separation of light hydrocarbons, ACS Appl. Mater. Interfaces 9 (16) (2017) 14506–14517.
[32] E. Andres-Garcia, J. López-Cabrelles, L. Oar-Arteta, B. Roldan-Martinez, M. Cano-Padilla, J. Gascon, G.M. Espallargas, F. Kapteijn, Cation influence in adsorptive propane/propylene separation in ZIF-8 (SOD) topology, Chem. Eng. J. 371 (2019) 848–856.
[33] E. Andres-Garcia, L. Oar-Arteta, J. Gascon, F. Kapteijn, ZIF-67 as silver-bullet in adsorptive propane/propylene separation, Chem. Eng. J. 360 (2019) 10–14.
[34] W. Liang, Y. Wu, H. Xiao, J. Xiao, Y. Li, Z. Li, Ethane-selective carbon composites CPDA@A-ACs with high uptake and its enhanced ethane/ethylene adsorption selectivity, AIChE J. 64 (2018) 3390–3399.
[35] X. Wang, Y. Wu, J. Peng, Y. Wu, J. Xiao, Q. Xia, Z. Li, Novel glucosamine-based carbon adsorbents with high capacity and its enhanced mechanism of preferential adsorption of C2H6 over C2H4, Chem. Eng. J. 358 (2019) 1114–1125.
[36] J. Kaurger, D.M. Ruthven, Diffusion in Zeolites And Other Microporous Solids, Wiley, New York, 1992.
[37] M. Khalighi, Y.F. Chen, S. Farooq, I.A. Karimi, J.W. Jiang, Propylene/propane separation using SiCHA, Ind. Eng. Chem. Res. 52 (2013) 3877–3892.
[38] C.Y. Lee, Y.-S. Bae, N.C. Jeong, O.K. Farha, A.A. Sarjeant, C.L. Stern, P. Nikias, R. Q. Snurr, J.T. Jupp, S.T. Nguyen, J. Am. Chem. Soc. 133 (2011) 5228–5231.
[39] R. Krishna, The Maxwell-Stefan description of mixture diffusion in nanoporous crystalline materials, Microporous Mesoporous Mater. 185 (2014) 30–50.
[40] R. Krishna, Methodologies for evaluation of metal-organic frameworks in separation applications, RSC Adv. 5 (2015) 52269–52295.
[41] R. Krishna, Screening metal-organic frameworks for mixture separations in fixed-bed adsorbers using a combined selectivity/capacity metric, RSC Adv. 7 (2017) 35724–35737, https://doi.org/10.1039/C7RA07363A.
[42] R. Krishna, Methodologies for screening and selection of crystalline microporous materials in mixture separations, Sep. Purif. Technol. 194 (2018) 281–300, https://doi.org/10.1016/j.seppur.2017.11.056.

Supporting information

Separation of C_3H_6 from C_3H_8 and N_2 by Ag(I)-doped Nanoporous Carbons Obtained from Hydrothermally Treated Lignin

Dipendu Saha[1], Marisa Comroe[1], Rajamani Krishna[2], Margaret Rascavage[1], Joel Larwa[1], Victor You[1], Griffin Standhart[1], Brandon Bingnear[1]

1 Department of Chemical Engineering, Widener University, One University Place, Chester, PA 19013, [2]Van't Hoff Institute for Molecular Sciences, University of Amsterdam, Science Park 904, 1098 XH Amsterdam, The Netherlands

Table S1. Langmuir-Freundlich fit parameters for C_3H_6, C_3H_8, and N_2 in Ag-C1 at 298 K.

	q_{sat} mol kg^{-1}	b $Pa^{-\nu}$	ν dimensionless
N_2	8	1.100E-07	1
C_3H_6	4	5.478E-03	0.47
C_3H_8	3.3	6.142E-03	0.49

Table S2. Langmuir-Freundlich fit parameters for C_3H_6, C_3H_8, and N_2 in Ag-C2 at 298 K.

	q_{sat} mol kg^{-1}	b $Pa^{-\nu}$	ν dimensionless
N_2	8	3.364E-07	1
C_3H_6	10	4.593E-03	0.5
C_3H_8	8.4	1.321E-03	0.6

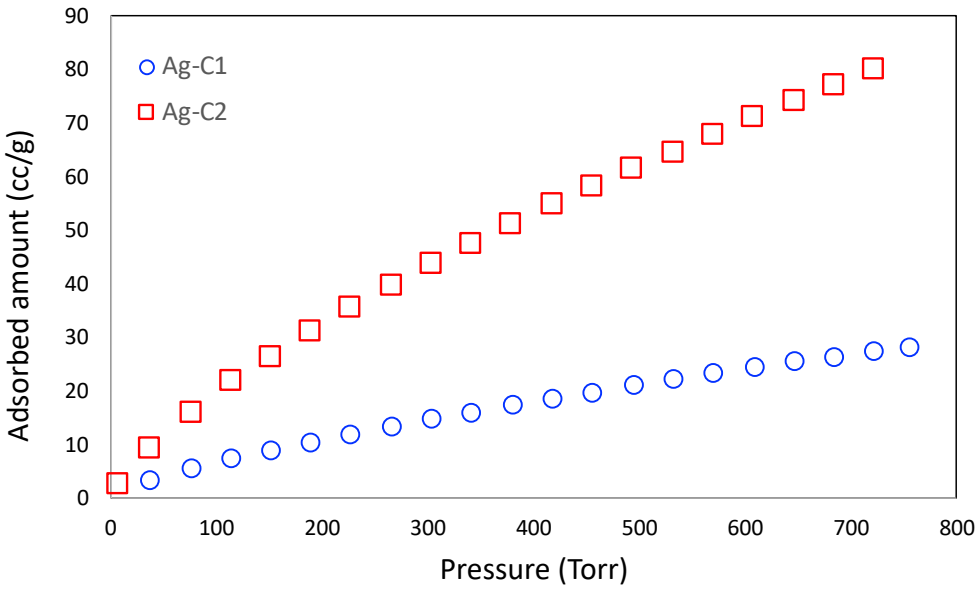

Figure S1. CO_2 adsorption isotherms on Ag-C1 and Ag-C2 at 273 K

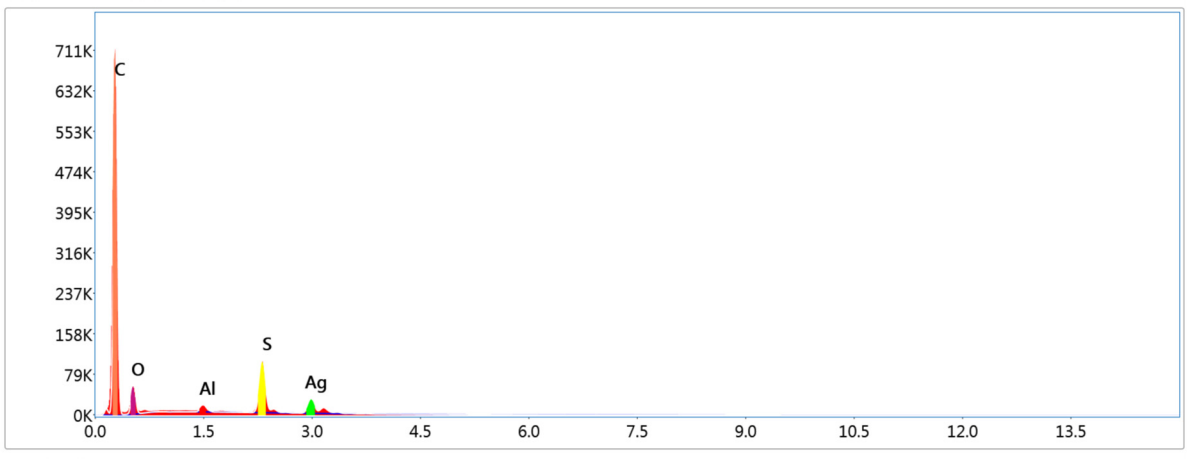

Figure S2. EDX spectrum of Ag-C2